

Formation of Single Gyroid Nanostructure by Order–Order Phase Transition Path in ABC Triblock Terpolymers

Tongjie Sun, Ping Tang,* Feng Qiu,* Yuliang Yang, and An-Chang Shi

The kinetics for the formation of the single gyroid (SG) nanostructure in ABC triblock terpolymers is investigated using the self-consistent field theory combined with the string method. Both simple phases (lamellae, cylinders, and spheres) and networked double diamonds (DD) can transform into SG through order–order phase transition (OOT). In particular, a packing frustration-induced variation in the epitaxial relationship between DD and SG is demonstrated. By regulating the block interaction, an expected epitaxial phase transition between these two networks without any rotation of the crystallographic directions can be achieved. Interestingly, the hexagonally perforated lamellae (HPL) are encountered in all identified transition pathways to SG. Nucleation kinetics investigation shows that the HPL tends to nucleate from SG easily, which confirms the kinetic origins of the instability of SG in experiments. Therefore, several strategies of preventing the SG being bypassed, such as controlling annealing time and rates during the morphology evolution, are proposed to promote the stabilizing of the SG in kinetic pathways. The findings reported here provide a novel route for fabrication of SG structured materials by manipulating both the epitaxial relationship and the nucleation kinetics in OOT pathways.

1. Introduction

As a relatively rare triply periodic cubic morphology, the single gyroid (SG, $I4_132$) has become a particularly fascinating structure due to its delicate geometrical characteristics and inherent chirality.^[1] It has been demonstrated that in certain butterfly wing scales, it is the SG network that produces the vivid structural colors.^[2] Natural butterfly wing scales offer an ideal route to investigate the optical properties of the gyroid structure, thus inspiring biomimetic technology.^[3] On the other hand, the self-assembly of block copolymer systems

provides a fairly promising means to generate 3D gyroid photonic crystals.^[1a,4] Block copolymers can self-assemble into a variety of multiply continuous network nanostructures, which can be classified into three categories: double network, single network, and alternating network.^[5] The double networks, including double gyroid (DG, $Ia\bar{3}d$), double diamond (DD, $Pn\bar{3}m$), and double plumber's nightmare (DP, $Im\bar{3}m$), contain two interpenetrating single networks formed by the same block of the copolymer. In contrast, the alternating networks, such as alternating gyroid (G^A , $I4_132$) and alternating diamond (D^A , $Fd\bar{3}m$), are composed of two intertwining and chemically distinct single networks.^[5c–f] The gyroid, diamond, and plumber's nightmare are threefold, fourfold, and sixfold connected networks, namely, each node of which is interconnected with three, four, and six struts or arms, respectively. The SG displays inherent left- or right-handed chirality not otherwise observed in any other

similar networked morphologies, thereby exhibiting linear and circular dichroism.^[1a,6] Single networks with 3D periodicity may exhibit a robust and complete photonic bandgap, thus meeting the demands of numerous optical applications.^[7] Additionally, they are also utilized for the manufacture of the metamaterials working at optical frequencies.^[8]

Although the double and alternating networks have been widely obtained in experimental observation and theoretical calculations, it remains a significant challenge to obtain SG by direct block copolymer self-assembly. However, the bottom-up self-assembly is still a fundamentally important means to manufacture SG structured materials. In fact, a variety of strategies have been developed with regard to the formation of the SG structure. The most general and effective means is to selectively etch one block of the G^A phase formed by triblock copolymers and backfill the resulting SG template with inorganic materials. After the removal of the remaining organic material, an SG networked structure will be obtained.^[1a,8,9] An alternative method is the coassembly of block copolymers with inorganic particles.^[10] Being utilized in the co-assembly processes, the amphiphilic block copolymers have become a significant class of structure-directing agents because of their selective interaction with certain inorganic nanoparticles. The whole block copolymer can be removed by etching or calcining, thus avoiding tedious processing steps and leading to the formation of single network.^[11]

T. Sun, Prof. P. Tang, Prof. F. Qiu, Prof. Y. Yang
State Key Laboratory of Molecular Engineering of Polymers
Collaborative Innovation Center of Polymers
and Polymer Composite Materials
Department of Macromolecular Science
Fudan University
Shanghai 200433, China
E-mail: pingtang@fudan.edu.cn; fengqiu@fudan.edu.cn
Prof. A.-C. Shi
Department of Physics and Astronomy
McMaster University
Hamilton, Ontario L8S 4M1, Canada

DOI: 10.1002/mats.201700023



Additionally, network shifting to achieve the transformation of the material properties from supergroup symmetry to subgroup symmetry proves to be a particularly appealing strategy recently. As a new class of networks with lower symmetry compared with conventional triply periodic cubic morphologies, shifted macroporous inorganic networks have been demonstrated to possess a complete bandgap.^[12] By network shifting means the SG, single diamond (SD), and single plumb's nightmare may be synthesized on the basis of diblock copolymer templates by simultaneously removing two single networks that are chemically indistinguishable and infiltrating the nanoporous matrix phase with precursors.^[13] Despite the progress, most of these methods are based on the alternating or double networks, which present various challenges for experimental procedures, including limitations on the choices of the copolymer templates or the inorganic nanoparticles and difficulties in realizing the transformation from double network to single network.

The order-order phase transition (OOT) provides a convenient platform for the manufacture of complex network mesophases with required long-range order and desired orientation.^[5g,14] However, to the best of our knowledge, there has been little theoretical or experimental work focusing on the OOT regarding the SG phase. Lately, the epitaxial intergrowth between DD and SG was reported on the basis of the stable inorganic replicas of silica scaffolds, which preliminarily revealed the possibility of the OOT between double and single networks.^[14a] In terms of this new route to the SG structure, there is a pressing need to further probe into its underlying mechanism. Nevertheless, the further experimental investigation about the formation of the SG seems to be an insurmountable challenge. First, in contrast to DG and G^A phases, SG phase, as yet, has never been demonstrated to be stable in pure block copolymer system. Exploiting various strategies to mitigate packing frustration, including the addition of conformationally ordered segments and appropriate homopolymers, can stabilize certain metastable double and alternating networks, such as DD^[15] and even the P phase.^[15e,16] Unfortunately, this strategy does not prove effective for the SG. Second, the addition of inorganic nanoparticles may result in a robust framework, as shown in the various fabrication routes for the SG mentioned above, along with those for numerous surfactant-directed mesoporous crystals.^[17] Though a complete photonic bandgap may be achieved by virtue of the high dielectric constant of those inorganic species,^[18] they prevent us from shedding light on the formation kinetics of the SG to a certain extent. Third, in terms of the gyroid photonic crystal materials, nucleation kinetics and the manipulation of the long-range order are two critical aspects to be considered,^[1a,19] which, however, are both relatively difficult to be elaborated via experimental procedures. Taking these factors into consideration, special attention should be paid to theoretical analysis for the formation of SG in kinetic pathways of the OOT.

Herein, we explore the kinetics for the formation of the SG phase in OOT pathways in ABC triblock terpolymers by employing the self-consistent field theory (SCFT) combined with the string method. The method has been successfully utilized to explore the free energy landscape and to obtain the OOT kinetics by evolving a string to converge to the minimum energy pathway (MEP) between two ordered phases.^[14d,20] With

regard to the SG structured materials, the unit cell size and the reciprocal lattice vectors are two critical factors associated with their applications.^[1a] Meanwhile, these two factors exactly determine the epitaxial relationship during the OOT between distinct phases.^[14d,20d,21] By investigating the matching relations of these two elements between varieties of morphologies and the SG, we aim to elaborate the epitaxial growth processes from various phases to SG. In particular, we demonstrate that the interconversion between DD and SG is possible to occur in purely polymeric systems. More importantly, their disparate responses to the variation of the interaction between end blocks may lead to distinct ratios of their unit cell sizes, and thus their epitaxial relationship varies. Taking advantage of this fact, one may achieve a straightforward phase transformation, i.e., an easier epitaxial intergrowth between DD and SG just by regulating the block interaction. The nucleation kinetics investigation reveals that the hexagonally perforated lamellae (HPL), which are encountered within the phase transition pathways from various phases to the SG, are easy to nucleate from the target phase SG. Therefore, we have suggestions on observing and stabilizing the SG in experiments. The findings reported here clarify the self-assembly of the SG in kinetic pathways and may provide important insights into the OOT route to other multiply continuous network nanostructures.

2. Theory and the Computation Method

The detailed derivation of the SCFT for linear ABC triblock terpolymers can be obtained from our previous investigation and the references therein.^[5c,22] The validity of the combination of the SCFT with the string method used to explore the OOT in block terpolymers has also been demonstrated in detail within our recent papers.^[14d,21] Thus, herein we just give a brief introduction to the main theoretical framework used in this study.

According to the SCFT, the free energy functional (F) of the system composed of n linear ABC triblock terpolymers in a volume V with the block compositions (the average volume fractions) being f_A , f_B , and f_C ($f_C = 1 - f_A - f_B$), respectively, can be expressed as

$$F/nk_B T = -\ln(Q/V) + (1/V) \int d\mathbf{r} [\chi_{AB} N\phi_A(\mathbf{r})\phi_B(\mathbf{r}) + \chi_{BC} N\phi_B(\mathbf{r})\phi_C(\mathbf{r}) + \chi_{AC} N\phi_A(\mathbf{r})\phi_C(\mathbf{r}) - \omega_A(\mathbf{r})\phi_A(\mathbf{r}) - \omega_B(\mathbf{r})\phi_B(\mathbf{r}) - \omega_C(\mathbf{r})\phi_C(\mathbf{r}) - \xi(\mathbf{r})(1 - \phi_A(\mathbf{r}) - \phi_B(\mathbf{r}) - \phi_C(\mathbf{r}))]$$
(1)

where $\phi_K(\mathbf{r})$ ($K = A, B$, and C) are the monomer density fields. The quantity Q is the partition function of a single chain subject to the mean field $\omega_K(\mathbf{r})$, and $\xi(\mathbf{r})$ is the potential field enforcing the incompressibility conditions. The immiscibility degrees between different blocks are characterized by the product $\chi_{AB}N$, $\chi_{BC}N$ and $\chi_{AC}N$, where N is the number of the statistical segments in a chain, and χ is the Flory-Huggins interaction parameter. In order to solve the functional integrals in the partition function, the saddle-point approximation is adopted to obtain the extremum of the integrand, namely by variations of F with respect to the monomer density fields and the potential fields; thus, the SCFT equations are derived. The

characteristic length scale of the ordered phase is presented in the unit of the radius of gyration of the block copolymer (R_g). The free energy for each phase can be divided into physically relevant contributions, interfacial energy and entropic energy, in which the entropic energy, $-TS$ can be written as

$$-TS/nk_B T = -\ln(Q/V) - (1/V) \int d\mathbf{r} [\omega_A(\mathbf{r})\phi_A(\mathbf{r}) + \omega_B(\mathbf{r})\phi_B(\mathbf{r}) + \omega_C(\mathbf{r})\phi_C(\mathbf{r})] \quad (2)$$

The different states obtained so can be used as the two ends of the string in the string method. The main objective of the string method is to obtain the minimum energy pathway (MEP) between the two states M and N on the energy landscape. The MEP is a curve or a string, ψ , in the configuration space connecting the two local minima of F . The MEP ψ satisfies the following equation

$$(\nabla F)^\perp(\psi) = 0 \quad (3)$$

where $(\nabla F)^\perp$ denotes the component of (∇F) normal to the string ψ . The free energies of the two states M and N are denoted by F_0 and F_1 , respectively. The MEP obtained is indicated as the evolution of $F - F_0$ along the string, i.e., the free energy difference between different discretized states along the string and the initial state M. The MEP $\psi(\alpha)$ connecting the two states M and N is parameterized by a variable α ($\alpha \in [0, 1]$) such that $\psi(0) = \phi_M$ and $\psi(1) = \phi_N$. In this paper, we have used two kinds of procedures to initialize the string. When we would like to obtain the possible metastable states formed during the OOT from M to N, the initial density distribution for each state needs to evolve gradually along the string in the whole calculation cell. In this way, we can simulate spinodal decomposition. On the other hand, to investigate the nucleation-growth mechanism, the states along the initial string will be set as a series of concentric spheres formed by the target structure growing gradually from the middle of the calculation box. After the initialization process, repeating the two procedures of iterating all the states along the string via SCFT and regulating the string using the difference method until the free energies for all the states along the string become constant, we ultimately obtain the MEP.

3. Results and Discussion

3.1. Epitaxial Intergrowth between Various Ordered Phases and SG

Epitaxial relationship, namely, the correspondence of the periodic structural elements between two morphologies, which exists extensively in OOT, originates from the matching of the dominant Fourier components.^[20d] As the primary wave vectors of DD are the {110} and the {111} family of the reciprocal lattice vectors, and those of the SG are {110},^[23] the interconversion between these two networks may be realized. Recently, the OOT between DD and SG has been observed in experiments by virtue of the inorganic structural analogies.^[14a] As a novel route to the SG phase, it provides a new understanding of the interconversion between double and single networks. However, further detailed investigation of the phase transition

between DD and SG is a tough task subject to the experimental conditions. Here, we will investigate their epitaxial relationship and analyze possible metastable morphologies involved in the OOT pathways using the SCFT combined with string method. We note the phase behavior in the C-rich corner of the triangle phase diagram of ABC triblock terpolymers where the typical structures with A core–B shell embedded in C matrix will be formed.^[5d]

Figure 1a displays one MEP between DD and SG, demonstrating the possibility of the OOT between DD and SG. Associated metastable morphologies indicated by the numbered arrows 1–7 in this kinetic pathway, are shown in Figure 1b1–b7 respectively. The thermodynamically stable phase at the condition is lamellae.^[5d] It can be seen that five metastable phases (except the two ends of the string) appear in the OOT pathway. Figure S1 (Supporting Information) shows their density distributions along the body diagonal on the (1–10) cross section to further detail their morphology evolution. Figure 1b2 shows that each node is stretched and distorted. Further stretching pulls apart a portion of the struts and leads to the perforated lamellae-like morphologies with different numbers of joints between each lamellae plane, which are shown in Figure 1b3,b4. Figure 1b5 displays the HPL morphology without any joints between distinct lamella planes. Reconnection and merging of the HPL finally result in the SG phase (Figure 1b7). Similar rearrangement of the nodes has been proposed in previous literatures as well.^[14a,24] These metastable morphologies might be easily observed in experiments due to the complexity of the experimental conditions. For example, in the recent experiments investigating the OOT between DD and SG, fluctuated and distorted structures have been observed at the boundary due to the solvent evaporation and the shift of the DD networks.^[14a] A large-amplitude mechanical shear could usually induce the formation of the HPL metastable states, while without shear, the perforated lamella-like morphologies with apparently poor spatial order can be obtained.^[25] In the OOT pathway shown above, the unit cell sizes of DD and SG are very close (with a small mismatch of 3%) which, however, is different from the recent experimental observation concluding that the ratio of the unit cell size between SG and DD is $\sqrt{2}/2$.^[14a] It has been confirmed that the matching of the unit cell size for distinct phases facilitates the epitaxial intergrowth process.^[5g,14d,20d,26] Matsen has demonstrated that a good match in the domain size between two phases, including cylinders and gyroid (with a only small mismatch of 2%)^[26a] as well as cylinders and spheres,^[26b] makes the epitaxial transitions easy to occur. In contrast, a large mismatch of the unit cell size requires a macroscopic transport of material and accordingly impedes the phase transitions. Distinct ratios of the unit cell size might lead to different epitaxial relationships. Although the variable epitaxial relationship between distinct phases has been discovered both experimentally and theoretically,^[20d,27] the variation mechanism is still an open question.

Figure 2a–c shows the density distribution of the three morphologies, DD (B shell), SG (B shell), and SG (A/B mixed) calculated in the same parameters, respectively. Subjected to the composition parameter ($f_A = 0.17$, $f_B = 0.25$, $f_C = 0.58$), the structures with A core surrounded by B shell embedded in the C matrix should be favored by the molecular topology, as

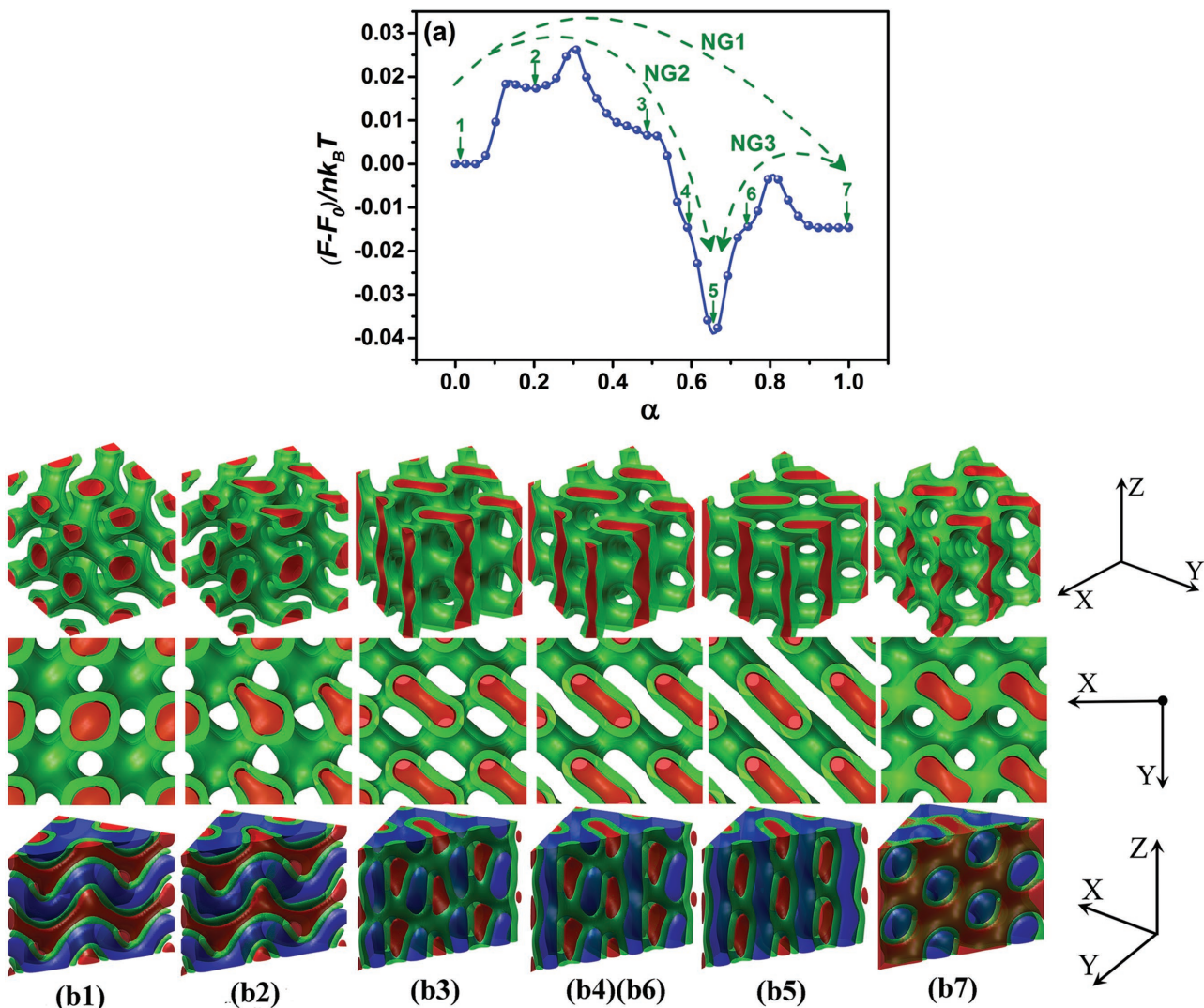


Figure 1. a) The MEP between DD (b1) and SG (b7) with $\chi_{AC}N = 35$, $\chi_{AB}N = \chi_{BC}N = 13$, and $f_A = 0.27$, $f_B = 0.25$, $f_C = 0.48$. The three possible nucleation and growth (NG) processes are indicated by NG1, NG2 and NG3, respectively. In addition, characteristic states along the string are indicated by the numbered arrows 1–7, and the corresponding intermediate morphologies are shown in panels (b1)–(b7). The first two rows show two-component morphologies (A and B phases) from different angles of view. The third row displays three-component morphologies (A–C phases) with (1–10) cross sections, and corresponding density distributions along the body diagonal are shown in Figure S1 (Supporting Information). Red, green, and blue represent A, B, and C domains, respectively.

shown in Figure 2a,b. However, it can be seen from Figure 2c that the SG (A/B mixed) possesses no obvious core–shell structural characteristics. Instead, A block and B block intermix with each other. This SG (A/B mixed) possesses a much smaller unit cell size of $4.4 R_g$, compared with that for DD (B shell, $7.2 R_g$) and SG (B shell, $6.8 R_g$). The formation of the SG (A/B mixed) can be attributed to the relatively weak interaction between A and C blocks, and accordingly the tendency to form A/C dispersive interface. To demonstrate this point, we have investigated the effect of the interaction between the end blocks on the unit cell size of DD and SG. As shown in Figure 3a, in the whole range of $\chi_{AC}N$ from 11 to 35, the variation of the interaction between the two end blocks A and C leads to different appearances of the SG and DD phases, including DD (semi-B shell), DD (B shell), SG (B shell), and SG (A/B mixed). As indicated

by the green box in Figure 3a, the SG (B shell) and the DD (B shell) show very similar unit cell size from $\chi_{AC}N = 19$ to $\chi_{AC}N = 35$ with the deviation no more than $0.4 R_g$ and their ratio is $L_{SG\text{ (B shell)}}/L_{DD\text{ (B shell)}} = 0.94\text{--}1.06$. In the red box when $\chi_{AC}N$ ranges from 19 to 27, both the SG (B shell) and the SG (A/B mixed) can be observed; however, the SG (A/B mixed) exhibits a much smaller unit cell size than the DD (B shell). Apparently, the epitaxial relationship between DD and SG in this range is possible to vary. When the $\chi_{AC}N$ decreases to the range from 11 to 17, the SG (A/B mixed) instead of the SG (B shell) can be obtained. With regard to the SG (A/B mixed) and the DD, the ratio of the unit cell size $L_{SG\text{ (A/B mixed)}}/L_{DD} = 0.56\text{--}0.79$. The recent experimental observation gave a ratio of $\sqrt{2}/2$ (0.707), which is within our calculation range.^[14a] Herein, the weak interaction between the end blocks A and C induces

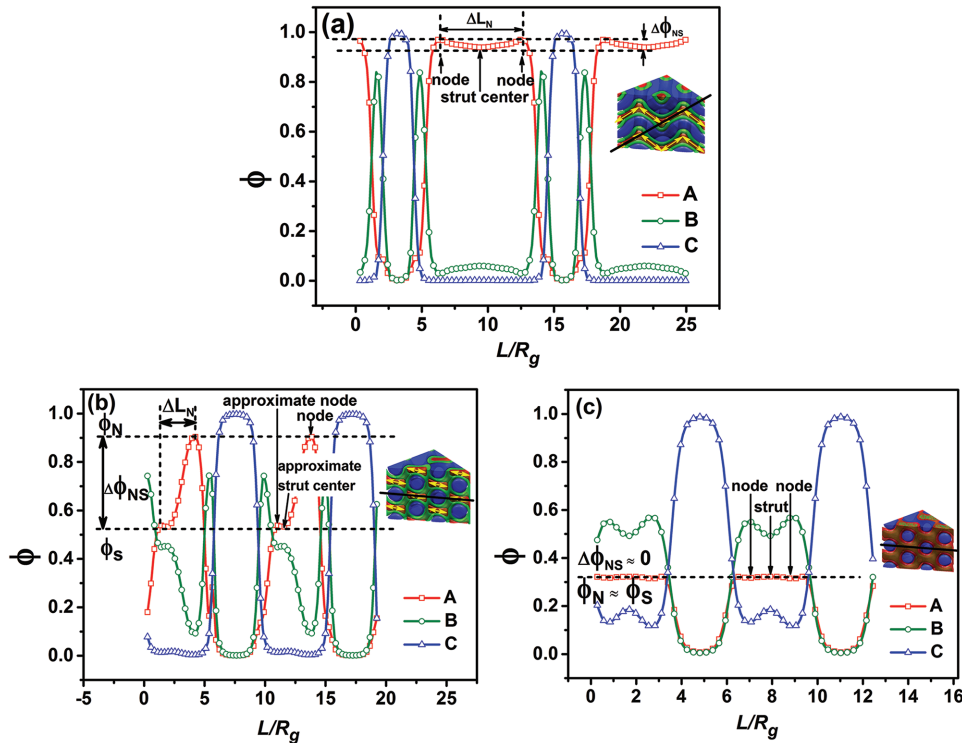


Figure 2. Density distribution of A–C blocks along the black line marked in the inset images, which are a) DD (B shell), b) SG (B shell), and c) SG (A/B mixed) with $f_A = 0.17$, $f_B = 0.25$, $f_C = 0.58$ and $\chi_{AC}N = 23$, $\chi_{AB}N = \chi_{BC}N = 35$.

the formation of A/C dispersive interface, thereby driving the system to form the phases with smaller unit cell size. In this case, the molecular chains would experience configurational change (Figure S2, Supporting Information). It can be seen from Figure 3a that the relatively weak interaction between the end blocks induces the formation of the SG (A/B mixed), while similar response does not happen to the DD (B shell), accordingly, leading to the significant difference of the unit cell size between DD and SG. This difference would give rise to the variation in the epitaxial relationship between DD and SG (Figure 3b). If the ratio of the unit cell size is between SG (A/B mixed) and DD is exactly $\sqrt{2}/2$ (the recent experimental result), then the SG (A/B mixed) phase prefers to rotate 45° to achieve epitaxial intergrowth with DD (B shell), as shown in Figure 3b. In this case, the epitaxial relationship between DD and SG is very similar to that between DD and DG.^[14e] Figure 3c,d shows that the [110] crystallographic direction of the DD (B shell) is parallel to the [010] direction of the SG (A/B mixed), while the [101] direction needs to rotate a certain degree α to transform into the [111] direction of the SG (A/B mixed). For the unit cell size of SG, reduction to the red box or increasing to the green box would not alter this favored epitaxial relationship. However, if the unit cell size of the SG equals that of the DD (the yellow box), then their epitaxial relationship would change remarkably. That is to say, there is no need for these two networks to rotate to achieve epitaxial intergrowth and all of the crystallographic directions coincide correspondingly, which makes the epitaxial intergrowth take place more readily. In short, the different responses of DD (B shell) and SG (B shell) to the variation in the interaction between end blocks lead to the big difference of

the unit cell size between these two networks, and accordingly the variation of the epitaxial relationship. What we will investigate further in the following part is the driving factors that trigger this distinct response.

In contrast to the surfactant systems with low molecular weight,^[14e,f,28] for the multiply continuous networked structures formed by block copolymers, however, packing frustration should be significantly considered.^[29] A large disparity in the domain thickness between the bulky nodes and the narrow connecting struts of the complex networks results in serious packing frustration. To mitigate this packing frustration, chain stretching favors domains of uniform thickness.^[4c,21,29,30] In view of this, we define two parameters to evaluate the degree of the packing frustration, i.e., the density difference between the node (ϕ_N) and the strut center (ϕ_S), $\Delta\phi_{NS} = \phi_N - \phi_S$, and the distance along the strut connecting two neighboring nodes, ΔL_N . Figure S3 (Supporting Information) illustrates the location of the node and strut for DD (B shell) and SG (B shell). As shown in Figure 2a,b, the density difference for A block between the node and the strut center $\Delta\phi_{NS}$ for SG (B shell), which is 0.374 , is much bigger than that for DD (B shell) which is 0.033 . The bigger density difference for the SG (B shell) reflects the fact that its domains are relatively nonuniform in thickness. This will lead to greater stretching mismatch between the bulky nodes and the narrow struts, i.e., more serious packing frustration.^[29a] In addition, given the similar unit cell size for DD (B shell, $7.2 R_g$) and SG (B shell, $6.8 R_g$), the longer distance between two neighboring nodes for DD (B shell), which is $6.2 R_g$, contributes to further relieving packing frustration. For the SG (B shell), however, ΔL_N is $2.89 R_g$. DD possesses

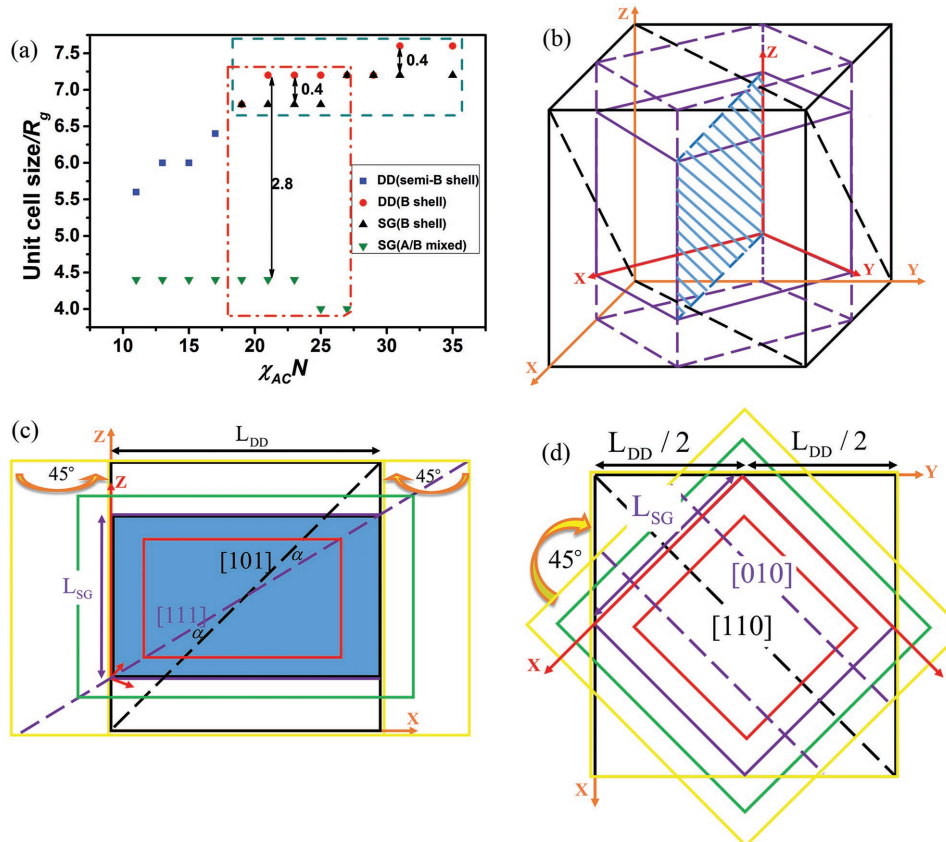


Figure 3. a) The unit cell size of DD (semi-B shell), DD (B shell), SG (B shell), and SG (A/B mixed) as a function of $\chi_{AC}N$ with $\chi_{AB}N = \chi_{BC}N = 35$ and $f_A = 0.17$, $f_B = 0.25$, $f_C = 0.58$. The green box indicates the range of similar unit cell size between DD (B shell) and SG (B shell). The red box indicates the coexistence range of the SG (B shell) and the SG (A/B mixed). Illustration of the variation in the epitaxial relationship between DD and SG. b) The rotation of the unit cell of SG along the common [001] axis with DD. The black cubic frame with orange coordinate axes represents the unit cell of DD; the purple one with red coordinate axes represents the unit cell of SG. The plane with blue lines represents the (1–10) plane of the SG, corresponding to the blue rectangle shown in part (c). The black dashed lines on the top and the bottom surface represent the [110] crystallographic directions, also shown in part (d) and those on the left and right surface the [101] directions, also shown in part (c). c) Projection along the [0–10] direction (the left view) of part (b). The purple dashed line represents the [111] crystallographic direction of the SG. d) Projection along the [001] direction (the top view) of part (b). Purple dashed lines represent the [010] crystallographic directions of the SG. The sizes of the purple and black box in parts (b)–(d) are indicated as L_{SG} and L_{DD} respectively, with $L_{SG}/L_{DD} = \sqrt{2}/2$. The red boxes in parts (c) and (d) represent the SG with smaller size; the green and yellow boxes with bigger size, in which the yellow ones have the same size with the black ones. When the size of the SG increases to that of the yellow box, the SG and DD boxes would coincide by rotating 45°.

two interpenetrating networks and SG just possesses one network, which further illuminates the weaker packing frustration for DD. Accordingly, the SG (A/B mixed) with weaker packing frustration arises. As shown in Figure 2c, the density difference $\Delta\phi_{NS}$ for A block of SG (A/B mixed) is almost zero, reflecting the attempt of the system to alleviate the serious packing frustration in the SG (B shell), which can be further confirmed by the obviously reduced unit cell size. In addition, the formation of A/C dispersive interface in SG (A/B mixed) makes the matrix formed by C block behave like “good solvent,” which further relieves the packing frustration. This packing frustration-induced variation in the epitaxial relationship is also in good agreement with the entropic contributions (Figures S4 and S5, Supporting Information).

According to the above analysis, by simply regulating the block interaction between end blocks, we can achieve an easier epitaxial phase transition between the two kinds of networked nanostructure DD and SG without the rotation of the

crystallographic directions. In fact, not only the DD, simple phases including lamellae, cylinders, and spheres can also transform into SG when following appropriate epitaxial relationship. Figure S6 (Supporting Information) shows that the domain sizes of DD and SG are very close to each other with a small mismatch of 3%. In addition, the lamellar structures with the (110) and (1–10) crystallographic planes which both belong with the {110} family, as well as the body-centered-cubic spheres (S^{BCC}) and [−1–11] hexagonally packed cylinders (C^{HEX}) all possess almost the same unit cell size as the SG (with a small mismatch of 3% between C^{HEX} and SG). However, the lamellae with other orientations, face-centered-cubic spheres (S^{FCC}) and tetragonally packed cylinders (C^{TET}) all have a large mismatch in the domain size with the SG (>20%). With the preferred epitaxial intergrowth relationship adopted, the epitaxial phase transition pathways and associate metastable states from lamellae, cylinders, and spheres to SG can be obtained (Figures S7 and S8, Supporting Information).

3.2. Emergence of HPL in Kinetic Pathways

Despite the emergence of various metastable morphologies in different pathways to the SG (Figure 1; Figures S7 and S8, Supporting Information), the HPL with $P6_3mmc$ symmetry (ABAB two-layer stacking), which can be referred to as HPLab, has always been discovered in all these identified pathways. Figure 4a1–a4 summarize four kinds of HPLab phases with various crystallographic planes of (110), (10–1), (1–10), and (101) formed in different OOT pathways from DD, lamellae, cylinders, and spheres to the SG phase. All of these crystallographic planes belong to the same {110} family of reciprocal lattice vectors. The corresponding HPLab phases are always more stable than the SG (Figure 4b), which might be a signal

that it would be easier to observe the HPLab with {110} directions rather than the SG in experiments. This will be analyzed in detail by nucleation kinetics investigation in the following section. In fact, the HPLab we obtained here has long been demonstrated in experimental observations.^[25a,31] As shown in Figure 4c, the d_1/d_2 ratio, which indicates the morphological characteristics of the HPLab phase, is 1.43, quite similar to the experimental results.^[25a] There is another intriguing phenomenon shown in Figure 4d1,d2 that the perforated lamellae (PL) with inhomogeneous holes (PLab) would appear before the formation of HPLab with homogeneous ones. Moreover, with increasing f_A , PLab with inhomogeneous holes becomes a metastable phase with higher barrier necessary for transforming into the HPLab. Below $f_A = 0.13$, the PLab may be observed as

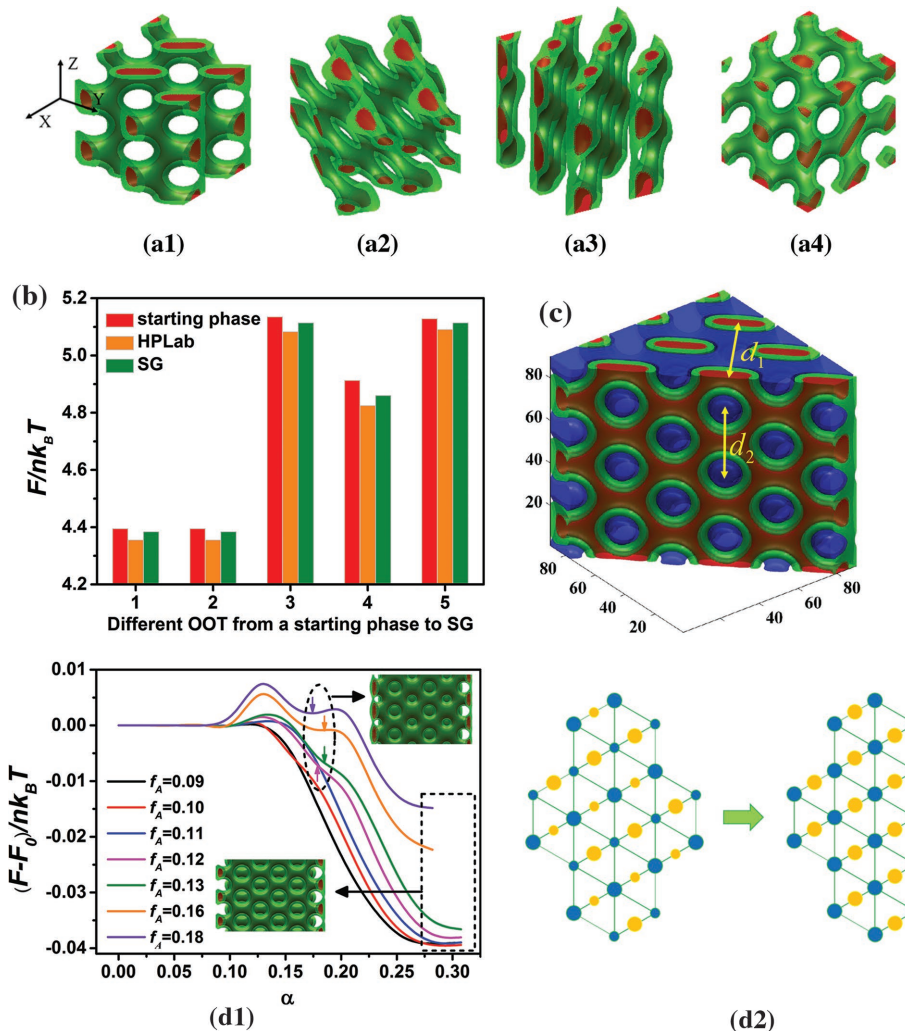


Figure 4. Formation of the metastable hexagonally perforated lamellae (HPLab) in the OOT pathways. [(a1)–(a4)] Four kinds of HPLab with crystallographic planes of (a1) (110), (a2) (10–1), (a3) (1–10) and (a4) (101). For their corresponding formation pathways see Figure 1 and Figures S7 and S8 in the Supporting Information. b) The comparison of the single chain free energy of different starting phases, corresponding intermediate HPLab and the ending phase (SG) in various OOTs from five starting phases to the SG. 1–5 indicate five OOTs which are (110) lamellae–SG, (1–10) lamellae–SG, [−1–11] hexagonally packed cylinders–SG, body centered cubic spheres–SG and DD–SG in corresponding compositions with $\chi_{AC}N = 35$, $\chi_{AB}N = \chi_{BC}N = 13$. The corresponding compositions for these five OOTs are $f_A = 0.1$, $f_B = 0.25$, $f_C = 0.65$, $f_A = 0.1$, $f_B = 0.25$, $f_C = 0.65$, $f_A = 0.27$, $f_B = 0.25$, $f_C = 0.48$, $f_A = 0.17$, $f_B = 0.25$, $f_C = 0.58$, and $f_A = 0.27$, $f_B = 0.25$, $f_C = 0.48$, respectively. c) The cross section of the (110) HPLab along the (110) directions; d_1 and d_2 indicate the repeat spacing perpendicular to the plane of lamellae and the spacing between two neighboring holes within the plane, respectively. d1) OOT pathways from (110) lamellae to (110) HPLab via an intermediate PLab with big and small holes simultaneously for a series of compositions at fixed f_B of 0.25. d2) The transformation from PLab with inhomogeneous holes to HPLab with homogeneous ones. Blue and yellow regions represent the holes in different planes.



a transient structure rather than a metastable one, which would be easy to grow into the HPLab. Although this PLab is inhomogeneous, there are actually just two types of holes with big and small diameters separately and arranging alternatively, which makes the PLab a possible metastable state in kinetic pathways. The PLab with alternating big and small sizes of holes would lead to a serious stretching mismatch of block A, giving rise to great packing frustration. The packing frustration would be alleviated by increasing f_A as the stretching is relieved with the increasing block length,^[29,30] and thus the PLab with inhomogeneous holes would become a metastable state, which may be observed in experimental procedures.^[25a]

3.3. Nucleation Kinetics for SG and HPLab

Nucleation, as a ubiquitous phenomenon in varieties of sciences, is the most general mechanism for phase transitions and closely linked to most of the OOT and order-disorder phase transition (ODT) processes.^[26,32] The real phase transition usually proceeds via nucleation and growth. Herein, based on the epitaxial relationship and the HPLab metastable state obtained above, we would analyze the nucleation kinetics for SG, particularly focusing on the nucleation processes between DD and SG. As shown in Figure 1a, the possible nucleation processes involving DD, SG, and the intermediate phase (HPLab) are indicated as NG1 (DD-SG), NG2 (DD-HPLab), and NG3 (SG-HPLab).

Figure 5a shows the specific nucleation pathways for NG1, NG2, and NG3. It should be mentioned that to simulate the phase transitions via a nucleation-growth mechanism, a large enough calculation box is required. Herein, to capture the nucleation process as accurately as possible, the system size is chosen to be 216 times that of the smallest cell. The free energy barriers per chain for these three nucleation processes are 4.93×10^{-3} , 1.25×10^{-3} , and $4.51 \times 10^{-4} k_B T$, respectively. It should be noticed that based on the free energy barrier per chain, true nucleation barriers of the system, which include all of the molecular chains, can be further calculated. Since the segment volume is Na^3 (a is the Kuhn length of the polymer segment) for a single molecular chain, the chain number in a critical nucleus is $\nu N^{1/2}/6^{3/2}$, where ν (in unit of R_g^3) is the volume of the critical nucleus. Assuming the degree of polymerization be 10^4 , the actual nucleation barrier of NG3, for example, is estimated to be $17.11 k_B T$. The free energy barrier per chain for NG1 is a little bigger than that for NG2. In other words, the nucleation barriers will prefer to choose the pathway from the DD to the HPLab rather than to the SG. This kinetic preference gives rise to a greater possibility to observe the HPLab instead of the SG. In spite of this, considering that the free energy barriers per chain for NG1 and NG2 are comparable, SG can still be obtained from DD. However, we notice that the nucleation barrier for NG3 is almost an order of magnitude lower than NG1. This is a hint that in the experiments, if we would like to observe a long-lived SG phase in the OOT pathway, the primary task should be to prohibit the further nucleation of HPLab from the obtained SG. It should be noticed that at the boundaries between the SG critical nucleus and the DD matrix shown in Figure 5b2, the nodes of the fourfold connected DD would be pulled apart to become the threefold junction of the SG, which is very similar

to the latest experimental observation.^[14a] In terms of other OOT such as from (110) lamellae to the SG, nucleation kinetics also shows that the SG is not a long-lived metastable state in kinetic pathways (Figure S10, Supporting Information).

Comparing the nucleation of SG with that of G^A and DG, we try to understand further the kinetic preference of the nucleation process. Figure 6 shows the kinetics regarding the OOT from the lamellar phase to DG and G^A, including the kinetic pathways for screening possible metastable morphologies and the nucleation processes. As shown in Figure 6a, the epitaxial relationship between the lamellar phase and the G^A is from (001) plane of the lamellae to (110) plane of the G^A. During this OOT process, there are no metastable states arising. Figure 6b displays the nucleation of G^A in (110) lamellar phase, with the critical nucleus morphology shown. The free energy barrier per chain decreases with increasing f_B , which is due to the system getting close to the ODT and the increasing obvious tendency toward spinodal decomposition. Figure 6c shows that the (12–1) planes of the core–shell DG are epitaxially related to the (001) planes of the lamellar phase, as is observed in diblock copolymers. The critical nucleus of the core–shell DG in (12–1) lamellae is shown in Figure 6d. There are two metastable phases encountered in the OOT pathways, including PL and cylinders corresponding to the two “valleys” in the MEPs. The PL phase is indicated in the green box in Figure 6c, which is not as stable as the DG phase. Accordingly, the nucleation of the PL in the DG phase is difficult to occur, while the DG can nucleate from the (12–1) lamellar phase via PL through a two-step nucleation mechanism.^[14d,20c] In contrast, as mentioned previously, the HPLab is relatively easy to nucleate from the SG phase, which reveals the kinetic origin of the instability of the SG in experiments.

According to the nucleation kinetics of SG and HPLab in kinetic pathways, we would try to propose several strategies in practical experiments to mitigate the current issue involving the competition between SG and HPLab. Due to the easier phase transition from the desired SG to the intermediate HPLab within the kinetic pathways, the primary task, as mentioned above, is to prohibit the nucleation of HPLab from SG and thus obtain a long-lived SG. First, we can regulate the annealing time of the phase transitions. A long enough period of time (like a week) is usually required to accomplish the phase transition to complex networked structures.^[5g,14b] However, in terms of the SG phase, annealing time needs controlling strictly by synchronous detection of the morphology evolution. Once the SG is formed, the systems need to be rapidly cooled to prevent the further nucleation of HPLab. Second, reducing heating or cooling rates would increase the probability of the emergence of the SG. Heating or cooling rates have been demonstrated to be a critical factor to affect the kinetic pathways to the DG phase.^[33] For the SG phase, due to the lower barrier of its phase transition to HPLab, it can easily be bypassed if the samples are heated or cooled too fast, thus resulting in the formation of HPLab. Third, by applying external fields such as oscillatory shear,^[34] pressure jump,^[35] and even electric fields^[36] to induce the phase transition as well as control the orientation of the cubic lattice, the SG phase may be easier to be observed. Compared with the OOT from DD to SG that from (110) lamellae to SG will not be easy to be stuck in the intermediate HPLab (Figure S10, Supporting Information). However, the barrier per chain for the

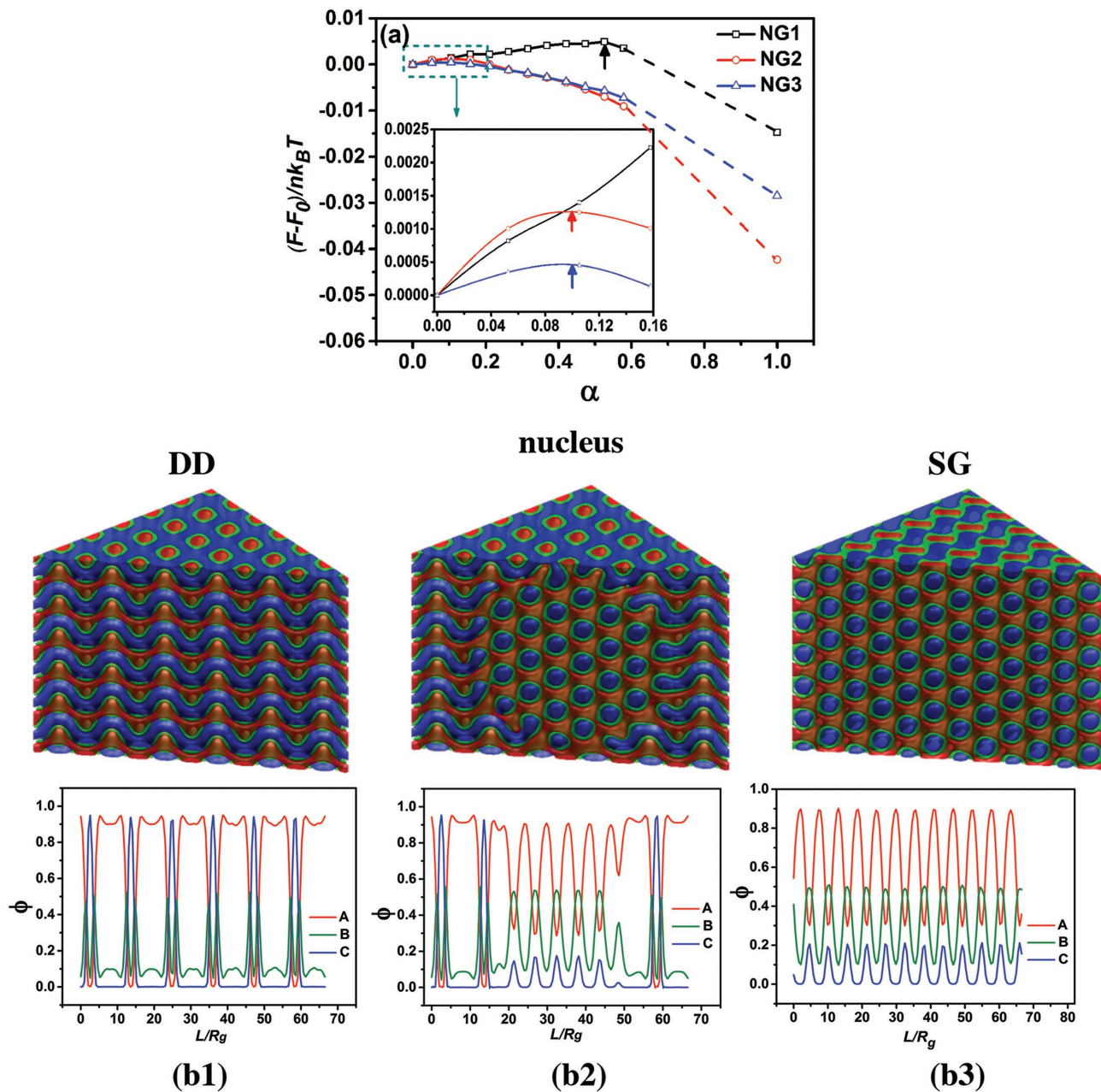


Figure 5. a) The MEPs for the nucleation of SG in DD (NG1), HPLab in DD (NG2) and HPLab in SG (NG3) with $\chi_{AC}N = 35$, $\chi_{AB}N = \chi_{BC}N = 13$ and $f_A = 0.27$, $f_B = 0.25$, $f_C = 0.48$. The nucleation pathways, NG1, NG2, and NG3, are also indicated in Figure 1a. The critical nucleus corresponds to the maximum of the free energy, as indicated by arrows with different colors. With regard to NG1, the cross section along the (110) crystallographic plane of DD, SG critical nucleus, and SG as well as corresponding density distribution along the body diagonal are shown in parts (b1)–(b3), respectively. The critical nuclei of HPLab in DD and in SG are shown in Figure S9b,c. Red, green, and blue represent A, B, and C domains, respectively.

phase transition of the latter (10^{-2}) is an order of magnitude higher than that of the former (10^{-3}) due to the obvious structural difference between flat lamellae and curved networks. Consequently, appropriate external fields would help to facilitate the transition from lamellae to SG. Fourth, by relieving the packing frustration, the SG might be stabilized in OOT pathways. Serious packing frustration remains an obstacle for stabilizing the complex network structures.^[15c,d,29a,37] To accomplish the stabilizing of complex ordered phases, various strategies have

been developed. Blending of the designed polymers (homopolymers or block copolymers) has proven to be an effective route to fabricate complex spherical packing phases (such as the Frank-Kasper phases^[38]), kaleidoscopic tiling patterns,^[39] as well as multiply continuous networks.^[15c-e,16] In addition, by adding inorganic nanoparticles, stable robust frameworks of the SG structure have been successfully created.^[8,13,14] Based on the OOT route shown in this study, these strategies would contribute to the experimental observation of the SG.

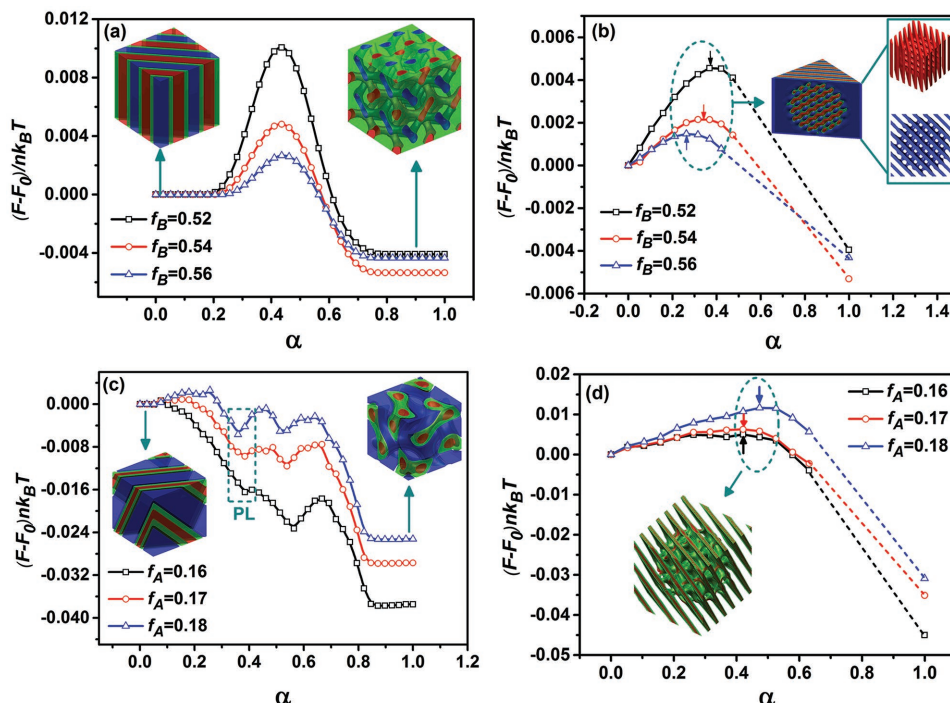


Figure 6. a) MEPs for screening possible metastable states during phase transition from (110) lamellar phase to G^A phase at different f_B with $f_A = f_C$ and $\chi_{AC}N = 35$, $\chi_{AB}N = \chi_{BC}N = 13$, b) corresponding nucleation of G^A in the lamellar phase. c) MEPs for screening possible metastable states during phase transition from (12-1) lamellar phase to DG phase at different f_A with $f_B = 0.25$ and $\chi_{AC}N = 35$, $\chi_{AB}N = \chi_{BC}N = 13$, d) corresponding nucleation of DG in the lamellar phase.

4. Conclusion

In the current work, the formation of the SG nanostructure in kinetic pathways of OOT in ABC triblock terpolymers has been investigated. Two kinds of epitaxial relationship between DD and SG are found, and a packing frustration-induced mechanism for the variation in the epitaxial relationship between these two networks is proposed. By regulating the monomer-monomer interaction to manipulate the epitaxial relationship, one may achieve an easier epitaxial intergrowth between DD and SG. Furthermore, the nucleation kinetics investigation reveals the kinetic origin of the instability of the SG in experiments and thus hints at the challenges of the fabrication of the SG via OOT in that the formation of the HPLab structure needs to be inhibited. Considering this, we have put forward specific strategies including regulating experimental conditions of phase transitions, such as controlling annealing time, slowing down heating or cooling rates, and applying external fields as well as adding appropriate polymers or nanoparticles, to guide the experiments to obtain the desired SG and to avoid the nucleation of the HPLab from the SG. The findings and interpretations reported here illuminate the epitaxial relationship and nucleation process regarding the SG nanostructure in kinetic pathways, and may provide important insights into the potential of the OOT route for engineering complex 3D periodic and functional networked nanostructures. According to the proposed principles of manipulating both the epitaxial relationship and the nucleation kinetics, one may achieve the fabrication of more affluent networked nanostructures with a

variety of potential applications through OOT paths, such as the transformation between DG and SD.

Supporting Information

Supporting Information is available from the Wiley Online Library or from the author.

Acknowledgements

The authors thank financial supports from the National Natural Science Foundation of China (Grant Nos. 21320102005, 21374023, and 21574027) and Ph.D. Programs Foundation of Ministry of Education of China.

Conflict of Interest

The authors declare no conflict of interest.

Keywords

double diamond, nanostructure, nucleation, phase transition, single gyroid

Received: March 22, 2017

Revised: May 27, 2017

Published online:

- [1] a) J. A. Dolan, B. D. Wilts, S. Vignolini, J. J. Baumberg, U. Steiner, T. D. Wilkinson, *Adv. Opt. Mater.* **2015**, *3*, 12; b) L. Wu, W. Zhang, D. Zhang, *Small* **2015**, *11*, 5004.
- [2] a) B. Winter, B. Butz, C. Dieker, G. E. Schröder-Turk, K. Mecke, E. Specker, *Proc. Natl. Acad. Sci. USA* **2015**, *112*, 12911; b) V. Saranathan, C. O. Osuji, S. G. Mochrie, H. Noh, S. Narayanan, A. Sandy, E. R. Dufresne, R. O. Prum, *Proc. Natl. Acad. Sci. USA* **2010**, *107*, 11676; c) A. Singer, L. Boucheron, S. H. Dietze, K. E. Jensen, D. Vine, I. McNulty, E. R. Dufresne, R. O. Prum, S. G. Mochrie, O. G. Shpyrko, *Sci. Adv.* **2016**, *2*, e1600149.
- [3] a) Y. Fu, C. A. Tippets, E. U. Donev, R. Lopez, *Wiley Interdiscip. Rev.: Nanomed. Nanobiotechnol.* **2016**, *8*, 758; b) Z. Gan, M. D. Turner, M. Gu, *Sci. Adv.* **2016**, *2*, e1600084; c) C. Mille, E. C. Tyrode, R. W. Corkery, *Chem. Commun.* **2011**, *47*, 9873; d) G. England, M. Kolle, P. Kim, M. Khan, P. Muñoz, E. Mazur, J. Aizenberg, *Proc. Natl. Acad. Sci. USA* **2014**, *111*, 15630.
- [4] a) A. M. Urbas, M. Maldovan, P. DeRege, E. L. Thomas, *Adv. Mater.* **2002**, *14*, 1850; b) M. Maldovan, A. M. Urbas, N. Yufa, W. C. Carter, E. L. Thomas, *Phys. Rev. B* **2002**, *65*, 165123; c) A. J. Meuler, M. A. Hillmyer, F. S. Bates, *Macromolecules* **2009**, *42*, 7221.
- [5] a) M. W. Matsen, *Macromolecules* **2012**, *45*, 2161; b) F. S. Bates, M. A. Hillmyer, T. P. Lodge, C. M. Bates, K. T. Delaney, G. H. Fredrickson, *Science* **2012**, *336*, 434; c) Z. Guo, G. Zhang, F. Qiu, H. Zhang, Y. Yang, A.-C. Shi, *Phys. Rev. Lett.* **2008**, *101*, 028301; d) J. Qin, F. S. Bates, D. C. Morse, *Macromolecules* **2010**, *43*, 5128; e) C. A. Tyler, J. Qin, F. S. Bates, D. C. Morse, *Macromolecules* **2007**, *40*, 4654; f) H.-H. Liu, C.-I. Huang, A.-C. Shi, *Macromolecules* **2015**, *48*, 6214; g) J. Suzuki, K. Nakane, A. Takano, Y. Matsushita, *Polymer* **2004**, *45*, 8989; h) J. Suzuki, M. Seki, Y. Matsushita, *J. Chem. Phys.* **2000**, *112*, 4862.
- [6] a) M. Saba, M. Thiel, M. D. Turner, S. T. Hyde, M. Gu, K. Grosse-Brauckmann, D. N. Neshev, K. Mecke, G. E. Schröder-Turk, *Phys. Rev. Lett.* **2011**, *106*, 103902; b) M. D. Turner, M. Saba, Q. Zhang, B. P. Cumming, G. E. Schröder-Turk, M. Gu, *Nat. Photonics* **2013**, *7*, 801.
- [7] a) C. Marichy, N. Muller, L. S. Froufe-Pérez, F. Scheffold, *Sci. Rep.* **2016**, *6*, 21818; b) J. A. Liddle, G. M. Gallatin, *ACS Nano* **2016**, *10*, 2995.
- [8] S. Vignolini, N. A. Yufa, P. S. Cunha, S. Guldin, I. Rushkin, M. Stefik, K. Hur, U. Wiesner, J. J. Baumberg, U. Steiner, *Adv. Mater.* **2012**, *24*, OP23.
- [9] a) S. Salvatore, A. Demetriadou, S. Vignolini, S. S. Oh, S. Wuestner, N. A. Yufa, M. Stefik, U. Wiesner, J. J. Baumberg, O. Hess, U. Steiner, *Adv. Mater.* **2013**, *25*, 2713; b) J. H. Moon, S. Yang, *Chem. Rev.* **2010**, *110*, 547.
- [10] B. P. Bastakoti, Y. Li, T. Kimura, Y. Yamauchi, *Small* **2015**, *11*, 1992.
- [11] a) M. Stefik, S. Wang, R. Hovden, H. Sai, M. W. Tate, D. A. Muller, U. Steiner, S. M. Gruner, U. Wiesner, *J. Mater. Chem.* **2012**, *22*, 1078; b) P. Docampo, M. Stefik, S. Guldin, R. Gunning, N. A. Yufa, N. Cai, P. Wang, U. Steiner, U. Wiesner, H. J. Snaith, *Adv. Energy Mater.* **2012**, *2*, 676.
- [12] L. Han, D. Xu, Y. Liu, T. Ohsuna, Y. Yao, C. Jiang, Y. Mai, Y. Cao, Y. Duan, S. Che, *Chem. Mater.* **2014**, *26*, 7020.
- [13] H.-Y. Hsueh, Y.-C. Ling, H.-F. Wang, L.-Y. C. Chien, Y.-C. Hung, E. L. Thomas, R.-M. Ho, *Adv. Mater.* **2014**, *26*, 3225.
- [14] a) X. Cao, D. Xu, Y. Yao, L. Han, O. Terasaki, S. Che, *Chem. Mater.* **2016**, *28*, 3691; b) H.-F. Wang, L.-H. Yu, X.-B. Wang, R.-M. Ho, *Macromolecules* **2014**, *47*, 7993; c) A. M. Squires, S. Akbar, M. E. Tousley, Y. Rokhlenko, J. P. Singer, C. O. Osuji, *Langmuir* **2015**, *31*, 7707; d) N. Ji, P. Tang, F. Qiu, A.-C. Shi, *Macromolecules* **2015**, *48*, 8681; e) A. M. Seddon, J. Hallett, C. Beddoes, T. S. Plivelic, A. M. Squires, *Langmuir* **2014**, *30*, 5705; f) T. Oka, *Langmuir* **2015**, *31*, 11353.
- [15] a) C.-Y. Chu, W.-F. Lin, J.-C. Tsai, C.-S. Lai, S.-C. Lo, H.-L. Chen, T. Hashimoto, *Macromolecules* **2012**, *45*, 2471; b) C. Chu, X. Jiang, H. Jinnai, R. Pei, W. Lin, J. Tsai, H. Chen, *Soft Matter* **2015**, *11*, 1871; c) M. W. Matsen, *Macromolecules* **1995**, *28*, 5765; d) M. W. Matsen, *Phys. Rev. Lett.* **1995**, *74*, 4225; e) F. J. Martínez-Veracoechea, F. A. Escobedo, *Macromolecules* **2009**, *42*, 1775.
- [16] a) P. Padmanabhan, F. Martinez-Veracoechea, F. A. Escobedo, *Macromolecules* **2016**, *49*, 5232; b) F. J. Martinez-Veracoechea, F. A. Escobedo, *Macromolecules* **2009**, *42*, 9058; c) T. Dotera, *Phys. Rev. Lett.* **2002**, *89*, 205502.
- [17] a) L. Han, K. Miyasaka, O. Terasaki, S. Che, *J. Am. Chem. Soc.* **2011**, *133*, 11524; b) Y. Zhao, L. Zhao, G. Wang, Y. Han, *Chem. Mater.* **2011**, *23*, 5250.
- [18] a) J. Yoon, W. Lee, E. L. Thomas, *MRS Bull.* **2005**, *30*, 721; b) M. Bockstaller, R. Kolb, E. L. Thomas, *Adv. Mater.* **2001**, *13*, 1783.
- [19] a) S. Peng, R. Zhang, V. H. Chen, E. T. Khabiboulline, P. Braun, H. A. Atwater, *ACS Photonics* **2016**, *3*, 1131; b) E. Goi, B. S. Mashford, B. P. Cumming, M. Gu, *Adv. Opt. Mater.* **2016**, *4*, 226.
- [20] a) W. E., W. Ren, E. Vanden-Eijnden, *J. Chem. Phys.* **2007**, *126*, 164103; b) L. Lin, X. Cheng, W. E., A.-C. Shi, P. Zhang, *J. Comput. Phys.* **2010**, *229*, 1797; c) X. Cheng, L. Lin, E. Weinan, P. Zhang, A.-C. Shi, *Phys. Rev. Lett.* **2010**, *104*, 148301; d) C. Wang, K. Jiang, P. Zhang, A.-C. Shi, *Soft Matter* **2011**, *7*, 10552; e) W. Li, P. F. Nealey, J. J. de Pablo, M. Müller, *Phys. Rev. Lett.* **2014**, *113*, 163801.
- [21] T. Sun, P. Tang, F. Qiu, A.-C. Shi, *Soft Matter* **2016**, *12*, 9769.
- [22] P. Tang, F. Qiu, H. Zhang, Y. Yang, *Phys. Rev. E* **2004**, *69*, 031803.
- [23] a) I. Y. Erkhimovich, *Eur. Phys. J. E: Soft Matter Biol. Phys.* **2005**, *18*, 383; b) K. Jiang, C. Wang, Y. Huang, P. Zhang, *Commun. Comput. Phys.* **2013**, *14*, 443.
- [24] A. M. Squires, R. H. Templer, J. M. Seddon, J. Woenkhaus, R. Winter, T. Narayanan, S. Finet, *Phys. Rev. E* **2005**, *72*, 011502.
- [25] a) L. Zhu, P. Huang, W. Y. Chen, X. Weng, S. Z. D. Cheng, Q. Ge, R. P. Quirk, T. Senador, M. T. Shaw, E. L. Thomas, B. Lotz, B. S. Hsiao, F. Yeh, L. Liu, *Macromolecules* **2003**, *36*, 3180; b) L. Zhu, P. Huang, S. Z. D. Cheng, Q. Ge, R. P. Quirk, E. L. Thomas, B. Lotz, J.-C. Wittmann, B. S. Hsiao, F. Yeh, L. Liu, *Phys. Rev. Lett.* **2001**, *86*, 6030.
- [26] a) M. W. Matsen, *Phys. Rev. Lett.* **1998**, *80*, 4470; b) M. W. Matsen, *J. Chem. Phys.* **2001**, *114*, 8165.
- [27] a) H.-W. Park, J. Jung, T. Chang, K. Matsunaga, H. Jinnai, *J. Am. Chem. Soc.* **2009**, *131*, 46; b) J. Jung, J. Lee, H.-W. Park, T. Chang, H. Sugimori, H. Jinnai, *Macromolecules* **2014**, *47*, 8761.
- [28] C. V. Kulkarni, *Nanoscale* **2012**, *4*, 5779.
- [29] a) M. W. Matsen, F. Bates, *J. Chem. Phys.* **1997**, *106*, 2436; b) J. Tang, Y. Jiang, X. Zhang, D. Yan, J. Z. Chen, *Macromolecules* **2015**, *48*, 9060.
- [30] Y. Gao, H. Deng, W. Li, F. Qiu, A.-C. Shi, *Phys. Rev. Lett.* **2016**, *116*, 068304.
- [31] Y.-L. Loo, R. A. Register, D. H. Adamson, A. J. Ryan, *Macromolecules* **2005**, *38*, 4947.
- [32] X. Xu, C. L. Ting, I. Kusaka, Z.-G. Wang, *Annu. Rev. Phys. Chem.* **2014**, *65*, 449.
- [33] M. E. Vigild, K. Almdal, K. Mortensen, I. W. Hamley, J. P. A. Fairclough, A. J. Ryan, *Macromolecules* **1998**, *31*, 5702.
- [34] a) M. Yamanoi, Y. Kawabata, T. Kato, *Langmuir* **2016**, *32*, 2863; b) A. M. Seddon, G. Lotze, T. S. Plivelic, A. M. Squires, *J. Am. Chem. Soc.* **2011**, *133*, 13860.
- [35] A. M. Squires, R. H. Templer, J. M. Seddon, J. Woenckhaus, R. Winter, S. Finet, N. Theyencheri, *Langmuir* **2002**, *18*, 7384.
- [36] C. W. Pester, C. Liedel, M. Ruppel, A. Böker, *Prog. Polym. Sci.* **2017**, *64*, 182.
- [37] M. W. Matsen, *J. Chem. Phys.* **1998**, *108*, 785.
- [38] M. Liu, Y. Qiang, W. Li, F. Qiu, A.-C. Shi, *ACS Macro Lett.* **2016**, *5*, 1167.
- [39] a) H. Miyase, Y. Asai, A. Takano, Y. Matsushita, *Macromolecules* **2017**, *50*, 979; b) K. Hayashida, T. Dotera, A. Takano, Y. Matsushita, *Phys. Rev. Lett.* **2007**, *98*, 195502.